A Machine Learning Based System for Multichannel Fluorescence Analysis in Pancreatic Tissue Bioimages

Julia Herold, Sylvie Abouna, Luxian Zhou, Stella Pelengaris, David B. A. Epstein, Michael Khan, Tim W. Nattkemper

Abstract— **Fluorescence microscopy has regained much attention in the last years especially in the field of systems biology. It has been recognized as a rich source of information extending the existing sources since it allows simultaneous collection of spatial and temporal protein information. In order to enable a high-throughput and high-content image analysis, sophisticated image processing routines become essential. We present a machine learning based approach for semantic image annotation i.e. identifying biologically meaningful objects. A semantic annotation becomes necessary, if image variables have to be associated to single biological objects, for example cells. We apply our method to pancreatic tissue sample images to detect and annotate cells of the Islets of Langerhans and whole pancreas. Based on the annotation, aligned multichannel fluorescence images are evaluated for cell type classification allowing accurate and rapid determination of the cell number and mass. This high-throughput analytical technique, requiring only few parameters, should be of great value in diabetes studies and for screening of new anti-diabetes treatments.**

I. INTRODUCTION

Over the past few years, various genome projects aiming at sequencing the whole genome of multiple organisms have been successfully carried out. Although many genes can be functionally annotated by wet lab experiments or using sequence similarity to annotated genes, for large numbers of genes, function is still unknown [1]. We are far from understanding how genomic information is interpreted during organism development, specialization etc. By studying the organism genomic sequence only, we are not able to tell where and when a specific protein will be expressed, to what function it will contribute and in which higher order network it will be embedded [2]. The field of proteomics, e.g. 2D gels etc., has focused on answering some of these questions but it lacks spatial information, i.e. at what location in a cell a protein is expressed and which other proteins are colocalized, because cell homogenization destroys this information. As has already been pointed out by Megason and Fraser [2] this is where imaging can play a significant role in further understanding how proteins contribute to cell function. It has the benefit of, for example, being able to capture quantitative data, offering subcellular resolution and by using fluorescence labeling, multiple proteins can be analyzed in the same sample making it possible to study patterns of colocalization. As an alternative to classical multichannel fluorescence imaging approaches [3], Schubert *et al.* [4] have introduced a new imaging technology, the Toponome Imaging System that enables the acquisition of images of hundreds of proteins on the same sample, overcoming the limitation of being able only to image few proteins at the same time. Due to developments in the field of bioimaging, an increasing amount of data needs to be analyzed, so that manual evaluation is no longer feasible.

In many applications of imaging in systems biology, it is necessary to restrict the analysis of image features, e.g. protein location, to biologically significant objects in order to reduce the amount of data to be analyzed and to enable a semantic interpretation of the information obtained. This semantic annotation can be, for example, identification of individual cells or cell compartments which is mostly achieved by intensity-, shape- or texture-based segmentation.

Depending on the object of interest, object characteristics can vary greatly, and it can thus be reasonable to introduce the concept of machine learning to the field of bioimage analysis. Using machine learning approaches like support vector machines (SVMs) [5], it is possible to learn object characteristics from a hand labeled set of samples. Providing the hand labeled set of image samples to tune the algorithm allows the biologists to apply their primary visual experience and expertise to the semantic annotation. SVMs have successfully been used in a variety of applications in the field of biological imaging. In e.g. [6] we showed how synapses only 3×3-5×5 pixels in size with very diffuse signals are detected via an SVM approach in fluorescence micrographs of neural tissue samples. Murphy *et al.* [7] have used SVMs for classification of fluorescence signals of different cell compartments, showing that structures of higher complexity can also be learned by an SVM if one chooses appropriate image features.

In this paper we demonstrate how machine learning based semantic annotation, in combination with multichannel fluorescence imaging, can be used to obtain information relevant to diabetes study and to screening of new anti-diabetes treatments. SVMs are applied for semantic annotation of cell nuclei of the Islets of Langerhans and whole pancreas in pancreatic tissue sample images. Based on the annotation

Manuscript received June 28, 2008

J. Herold and T. W. Nattkemper are with the Faculty of Technology, Biodata Mining & Applied Neuroinformatics Group, University of Bielefeld, 33615 Bielefeld, Germany (+49 521 106 6067; {jherold, tnattkem}@techfak.uni-bielefeld.de)

S. Abouna, L. Zhou, and M. Khan are with the Biomedical Research Institute, Department of Biological Sciences, University of Warwick, Coventry CV4 7AL, UK ({s.s.abouna, luxian.zhou, michael.khan}@warwick.ac.uk)

S. Pelengaris is with the Medical School, University of Warwick, Coventry CV4 7AL, UK (stella.pelengaris@warwick.ac.uk)

D. B. A. Epstein is with the Mathematics Institute, University of Warwick, Coventry CV4 7AL, UK (david.epstein@warwick.ac.uk)

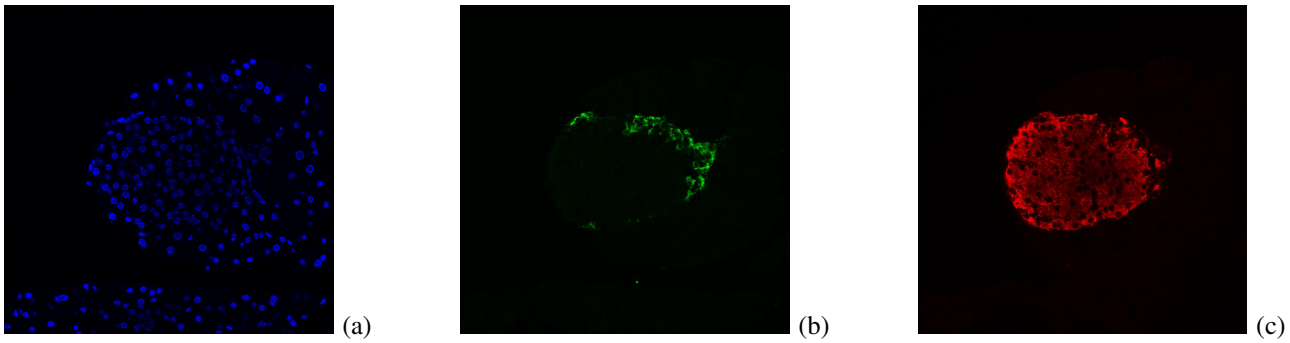

Fig. 1. 512×512 px sized pancreatic tissue sample images stained with (a) DAPI showing cell nuclei, (b) immunostained for glucagon showing α-cells and (c) immunostained for insulin showing β-cells.

result two additional fluorescence images of the same tissue are evaluated to identify islet specific alpha and beta cells.

Increasingly, researchers are interested in the ratio or balance of alpha and beta cells as type 2 diabetes, which affects around 200,000,000 people worldwide, is primarily caused by a defective number of beta cells, which produce the sugar lowering hormone insulin. However, excess of alpha cells and glucagon production, which raise glucose, may contribute to hyperglycaemia. Also current drugs may partly work by reducing glucagon.

II. MATERIAL

Images are obtained by confocal microscopy with a ×40 objective. Each tissue section is immunostained for two proteins, namely insulin and glucagon. Insulin is produced by beta cells (β-cells) and glucagon by alpha cells (α-cells), so this staining enables us to identify and distinguish these different cell types. In addition we use DAPI (4',6-Diamidino-2-phenylindol) which stains DNA blue irrespective of the cell type. As an example fig. 1 displays the images obtained for one tissue sample. 1(a) shows the staining with DAPI displaying nuclei, 1(b) α-cell immunostaining for glucagon and 1(c) β-cell immunostaining for insulin.

III. METHODS

In the following section we present our pipeline for semantic image annotation and multichannel image analysis. Fig. 2 outlines the different steps. First, fluorescence imaging is used to acquire multiple protein channels for each biological sample, i.e. each protein channel represents one fluorescently marked protein in the same sample (fig. 2 step 1.). In order to restrict all further analysis to biologically meaningful regions or objects, a semantic image annotation is carried out by SVM classification of one or more images (fig. 2 step 2.). Based on the semantic annotation, additional channels are analyzed and the objects extracted in step 2. can, for example, be assigned to different object classes, here red, blue, green and yellow, based on the underlying multichannel characteristics. To this end, for each detected cell nucleus a region of interest (ROI) is computed.

A. Image preprocessing

For noise reduction bilateral filtering [8] is applied. The geometric spread parameter σ_d can be fitted based upon the

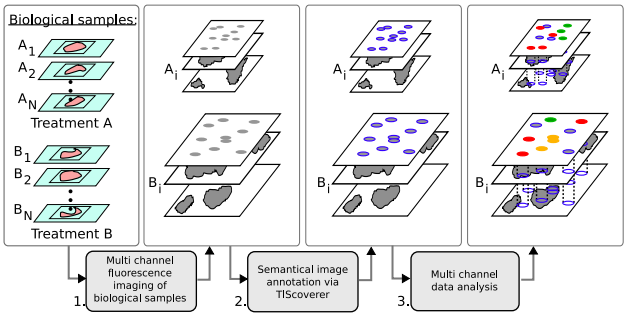

Fig. 2. Evaluation pipeline for multichannel fluorescence image analysis. After acquisition of multiple protein channels via fluorescence microscopy (1.) images are semantically annotated (2.). Regions of interest (ROI) are shown in blue. Restricted to the ROIs, multiple other channels can be analyzed. ROIs can then be e.g. classified in different object classes, here red, blue, green, yellow.

maximum object size (N_{max}) measured in pixels, in our case the maximum nucleus size N_{max}=17 pixels. Thus the geometric spread is set to $\sigma_d = \frac{N_{max}-1}{4}$. The photometric spread is set to σ_r= 20. These values have proven to be appropriate values for noise reduction in the images analyzed.

B. Semantic Image Annotation

A support vector machine approach is applied for semantic image annotation, i.e. localizing biologically meaningful objects in the image, in our case cell nuclei stained with DAPI. Therefore $N \times N$ ($N = N_{max}+2$) sub-images-images (patches) of the image are classified. Patches containing a nucleus are to be classified as nuclear patches, and other patches are assigned to the non-nuclear class. The patch size is chosen based upon the maximum nucleus size and adding a small border in order to include background pixels even for very large nuclei.

As a SVM is a supervised learning approach, a training set containing positive and negative samples is necessary for SVM training. Therefore, an image of nuclei is manually evaluated by a human expert labeling an equal number of positive and negative training samples. For each nucleus position contained in the training set the gray values of the $N \times N$ neighborhood are written to a N^2 dimensional gray value feature vector. As we assume that the samples are invariant with respect to rotation we increase the training

set fourfold by rotating each patch four times by an angle of $\beta = k * \frac{360^\circ}{4}$ with $k = \{0, 1, \ldots, 3\}$.

For SVM training the dimensionality of the feature vectors is reduced to 8 dimensions by applying a PCA projection onto the first 8 eigenvectors with highest eigenvalues. This has the benefit that less time is needed for SVM training and fewer training samples are required. Training is performed with a Gaussian kernel where kernel parameterization is achieved through a fully automatic 10 fold cross validation.

To localize nuclei in a whole micrograph, for each image location p, its $N \times N$ gray value feature vector is extracted, a PCA projection is performed and the resulting feature vector is classified by a trained SVM. If the patch is classified as nuclear, the confidence value, i.e. distance to the hyperplane, is written to position p of a new matrix of the same size as the original image. This *confidence map* is subsequently evaluated to obtain nucleus positions. High confidence areas correspond to nucleus locations where the highest value is likely to be the nucleus centerpoint. We therefore search for local optima exceeding a confidence threshold t within a $N_d \times N_d$ ($N_d = \frac{N-1}{2}$) neighborhood where N_d accounts for the minimal distance between two separate objects. These positions are interpreted as nucleus center positions.

If a gold standard for an image is available, performance measures as sensitivity (SE) or positive predictive value (PPV) can be calculated for the detection result obtained by the SVM. Here, SE measures the percentage of nuclei given in the gold standard which are also detected by the SVM. PPV accounts for the percentage of detected nuclei which are also contained in the gold standard. To obtain a gold standard, all nuclei of an image are manually labeled by a human expert.

C. Multichannel Analysis

Once an image has been semantically annotated, further channels, i.e. different labeled proteins, can be analyzed and evaluated restricted to the ROIs. In the image domain used throughout this paper, two additional channels are available which are used to classify a nucleus as an α-, β- or non-islet-cell nucleus depending on the observed fluorescence signal of the additional channels surrounding the nucleus.

To obtain ROIs, nucleus borders are extracted as a first step. Therefore, at each nucleus position, obtained by the semantic annotation, an image patch of size $N_{max} \times N_{max}$ is extracted, a gray value morphological closing is performed and the image is thresholded via Otsu thresholding [9]. The nucleus border can be obtained by a two fold dilation of the thresholded image and subtracting the original thresholded image from the dilated. See fig. 3(a) for the extraction of a nucleus border.

Based on the nucleus segmentation, two strategies to analyze the remaining channels for nucleus classification can be applied:

1. α- and β-channels are separately thresholded via Otsu thresholding into background and object pixels. For each nucleus, we calculate the border coverage, i.e. percentage of nucleus border pixels, extracted in the previous step, which are object pixels in the α- and β-channel, as c_α and c_β respectively. See fig. 3(b) for an example. If $c_\alpha \geq t_{p\alpha}$ or $c_\beta \geq t_{p\beta}$, with $t_{p\alpha}$ and $t_{p\beta}$ being user defined thresholds, the nucleus is classified as α- or β-cell nucleus, respectively. Any nucleus classified neither as α- nor as β-cell nucleus is classified as non-islet-cell nucleus. Thresholding the different channels furthermore gives information about the percentage of α- and β-cell mass with respect to the whole islet cell mass which can be determined by merging the thresholded α- and β-channels and counting all object pixels.
2. A median intensity is calculated for α- and β-cell channels for the nucleus border pixels, as shown in fig. 3(c). If the median intensity is above a user defined threshold $t_{i\alpha}$ or $t_{i\beta}$ the nucleus is classified as α- or β-cell nucleus, respectively. The remaining nuclei are classified as non-islet-cell nuclei.

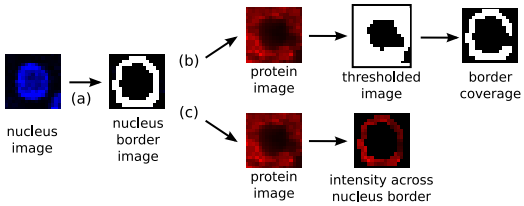

Fig. 3. Multichannel analysis. After extraction of the nucleus border (a), two strategies can be applied to analyze the different protein channels. (b) Each channel is separately thresholded and the overlap of border image and thresholded image is analyzed. (c) The overlap of the protein image and border image is analyzed and the median intensity of the border is calculated.

A gold standard for the α- and β-cell nucleus number is obtained by a fourfold manual evaluation of the different channels. The average over all four counts is used as the gold standard.

D. Software

All the above mentioned steps for semantic annotation including manual image labeling, training set generation, SVM training as well as image classification and confidence map evaluation are implemented in C++ in our own software *TIScoverer 1.0*. It also allows non computer experts to perform object detection via SVM while still offering a reasonable amount of manual tuning if desired. Fig. 4 shows screenshots of the *TIScoverer 1.0* software. The label environment is shown in 4(1.) displaying all labels set in the image, with green marking positive samples and red marking negative samples, and an enlarged view of the current active label allowing a precise determination of position. 4(2.) gives an overview of the SVM training environment. The training image and a training file containing human expert label positions can be loaded, a PCA projection can be performed and a few parameters, e.g. patch size and names of output files, are then set. Fully automatic training runs and training performance can subsequently be evaluated. The detection result for a newly presented image is shown in fig. 4(3.).

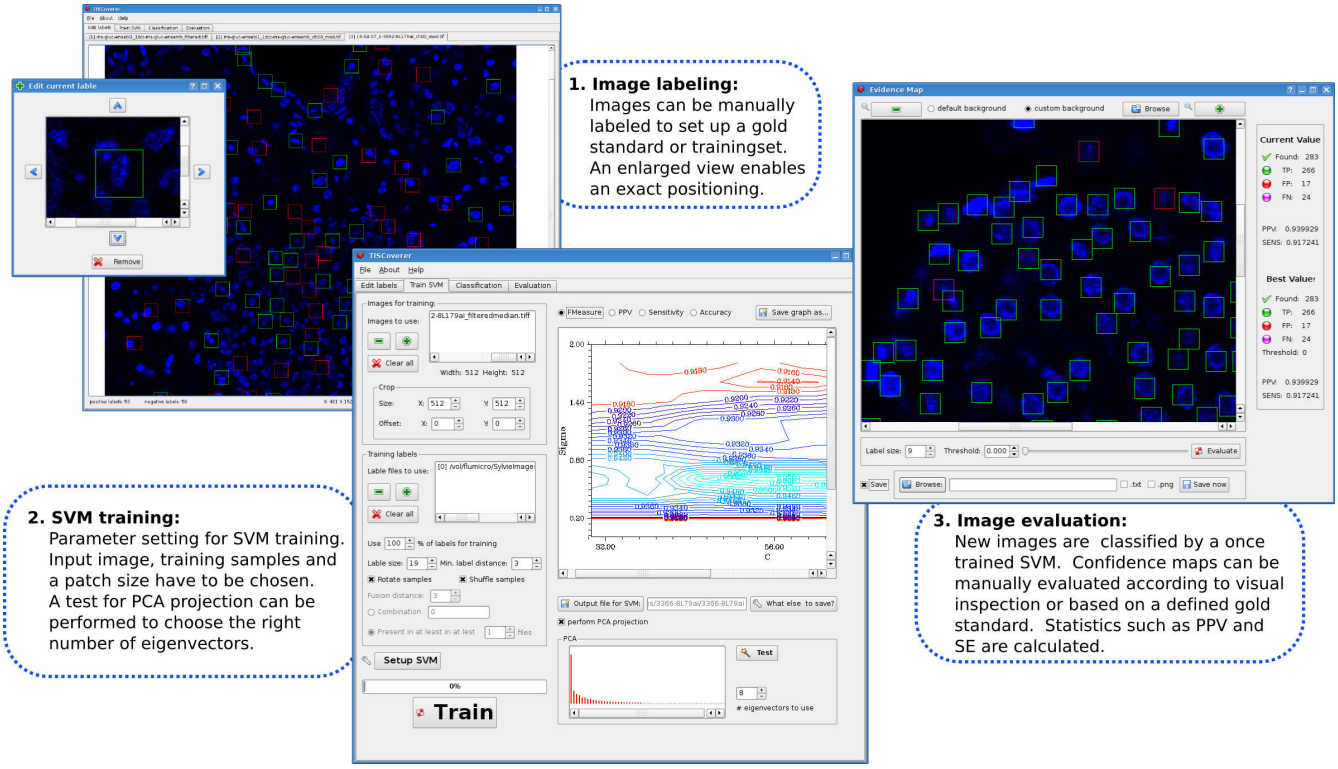

Fig. 4. Screenshots of TIScoverer software. 1. shows the label environment allowing one to set up training sets or gold standards. An enlarged view of the current active label enables accurate positioning. 2. Training is performed by selecting input image, training samples and some parameters. A full automatic cross validation selects best parameters for kernel parameterization. 3. Detection results can be visually and statistically evaluated.

Rectangles show the detected nucleus positions and color coding gives information about true positives (TP)(green), false positives (FP)(red) and false negatives (FN)(pink). Also statistics such as SE and PPV, as well as the whole number of detected nuclei are presented at the right side.

IV. RESULTS

In the following we present the results obtained for nucleus detection, i.e. semantic annotation, and multichannel analysis. By way of example, results are presented for two tissue sample images.

A. Nuclei detection

For nucleus detection, we perform a SVM training with a Gaussian kernel on a tissue sample image stained with DAPI (image not shown) with a hand labeled training set consisting of 59 positive and 59 negative samples. The trained SVM is then used for nucleus detection in the image in fig. 1(a).

To assess the automatic detection performance on the image, we calculate SE and PPV for the SVM detection result obtained for different confidence thresholds. The best detection results is obtained with a confidence threshold of 0.0, which is true also for detections in other images, yielding 283 detected nuclei with a SE of 92% and PPV of 94%. The detected nuclei are marked in fig. 5(a) with a rectangle where TP are shown in white, FP in red and FN in orange. An enlarged view of the detection result is shown in 5(b) for better visibility of overlapping nuclei, FPs, and FNs, which are mostly out of focus nuclei of poor quality.

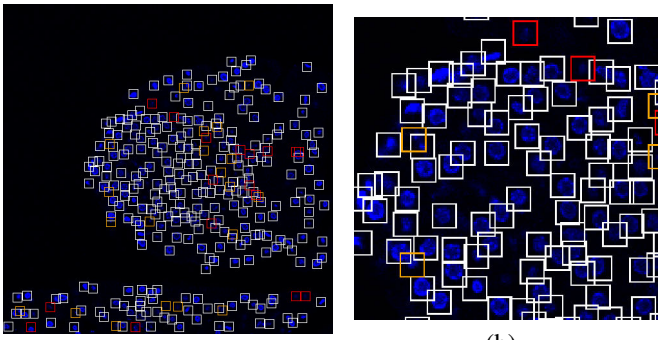

(a) (b)

Fig. 5. Nucleus detection results for the image shown in fig. 1(a). Detected nuclei are highlighted with a rectangle (white TP, red FP, orange FN). (b) Enlarged view of the detection result. Overlapping nuclei and non regularly shaped nuclei are correctly detected.

B. Cell type classification via multichannel analysis

For each nucleus position obtained by the semantic annotation its boundary is extracted based on the DAPI stained image. Fig. 6(a) and 6(b) show the extracted nucleus boundaries in white for fig. 1(a) and for a second tissue sample, respectively. Fig. 6(c) and 6(d) show overlapping nuclei. The boundaries overlap at their intersection point as can be seen by the lighter gray boundary color. This information could

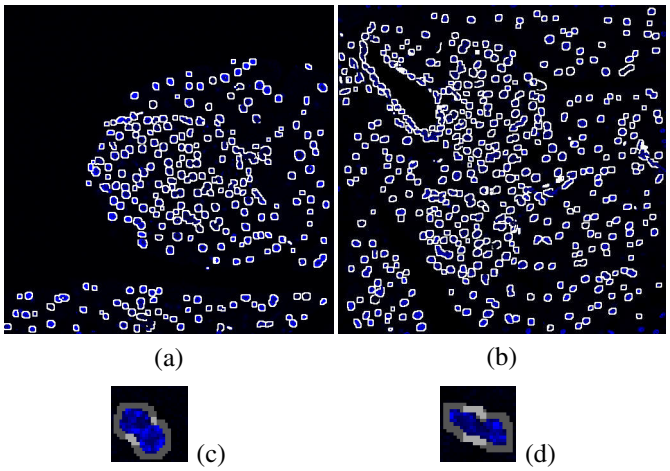

Fig. 6. Extracted nuclei borders, shown in white, with (a) for the image of fig. 1(a) and (b) for a second tissue sample. (c) and (d) show sub-images displaying two overlapping nuclei.

be used to separate nucleus boundaries if required.

After nuclei boundary extraction, α- and β-channel images can be analyzed for each nucleus. The first strategy presented, i.e. Otsu thresholding and boundary coverage analysis, allows us to analyze different protein channels based on a biological model, e.g. a nucleus has to be surrounded by stained cytoplasm to a specific minimum percentage. Fig. 7(a) shows the percentage of α-channel border coverage vs. β-channel border coverage for each nucleus detected in 5(a). Setting the coverage threshold to 45% for the α- and to 60 for the β-channel (fig. 7(b)) yields 102 (35%) cell nuclei classified as cell nuclei of β-cells and 22 (8%) classified as α-cell nuclei, with an overlap of 10 nuclei classified both as α- and β-cell nuclei. The nuclei classified both as α- and β-cell nuclei are only counted as α-cell nuclei thus yielding 92 (33%) β-cell nuclei and an α- to β-cell ratio of 0.24. This quite well agrees with the manual counting of an average of 91 β-cell nuclei and 24 α-cell nuclei. The cell masses calculated are 12% for the α-cells and 88% for the β-cells with respect to the whole islet cell mass.

Fig. 8 presents the classification result with 8(a) showing a blending of the nucleus- and α-channel where α-cell nuclei are highlighted with a white box and 8(b) displaying a blending of the nucleus- and β-channel with β-cell nuclei highlighted with a white box. Fig. 8(c) and 8(d) show equivalent results with the same thresholds for the second tissue sample, yielding 23 (4%) α-cell nuclei and 110 (21%) β-cell nuclei (α- to β-cell ratio: 0.21) with 14% α-cell mass and 85% β-cell mass. The average manual count is 40 α-cells and 100 β-cells. The disagreement between human and machine counting of β-cells is caused by the fact that also cells featuring no nucleus were manually counted.

The analysis strategy mentioned before might not always lead to the desired result as it is based upon binarizing the image via Otsu thresholding which might not always reflect the true underlying structure. We therefore also compute the median intensity value across the nucleus border. This implicitly accounts for a border coverage of 50% with the median as the intensity threshold. Fig. 7(c) shows the median α-channel border intensity vs. the median β-channel border intensity for each nucleus with logarithmic scaling. This figure suggests an intensity threshold of 20 for the β-channel and a threshold of 15 for the α-channel in order to separate β- and α-cell nuclei from non-islet-cell nuclei. By looking more closely at the classification results for these thresholds (data not shown), one can see that there are some nuclei assigned to the β-cell nuclei class which do not meet the desired characteristics. Adjusting the threshold to 30 for the β-channel, classification results close to the manual counting can be obtained as can be seen in fig. 8(c) and 8(d) with 23 (8%) of the total of nuclei detected being classified as α-cell nuclei and 92 (33%) as β-cell nuclei (α- to β-cell ratio: 0.25). Fig. 8(g) and 8(h) show results for the second tissue sample, with a threshold of 15 for the α-channel and 35 for the β-channel yielding 28 (5%) of all nuclei classified as α-cell nuclei and 101 (20%) as β-cell nuclei (α- to β-cell ratio: 0.27). This strategy gives slightly better results than the previous strategy but is not as intuitively tunable as the border coverage strategy.

V. DISCUSSION

We have given here an approach to working with multi-channel microscope images by applying a machine learning strategy for semantic image annotation. Only few parameters are required for the training of a SVM detecting cell nuclei. First, the maximum object size N_{max} needs to be set, from which further parameters (N, N_d) can be derived. Second, the target dimensionality for PCA projection has to be specified—this can easily be determined by analyzing the eigenvalues which are displayed in *TIScoverer 1.0*. Furthermore, a training set needs to be declared. In the analyzed case a training set consisting of few representative samples (59 positive and 59 negative samples) is already sufficient to achieve good detection results in various images. Once the SVM has been trained, no further parameters need to be specified. This low number of parameters and training samples required makes the software easily usable also by non computer experts but at the same time allows for manual tuning if desired. As SVMs have successfully been used for the classification of more complex structures, an extension of the system beyond structures as simple as cell nuclei should be achievable.

Based on the semantic annotation, further channels, not limited to α- and β-channels, can selectively be evaluated and already very simple image processing approaches give high quality results. Again, only few parameters, i.e. border coverage in each channel or median intensity in each channel, need to be specified. Setting these parameters is crucial for the classification outcome but can be aided by visualizations as shown in fig. 7 and by real time update of the resulting classification visualization when parameters are changed.

The whole process of semantic annotation with a trained SVM and multichannel analysis only requires around 20 seconds on an INTEL Core 2 Duo CPU with 3 Ghz and 2 Gb RAM, and it is sufficient to set 2 parameters which

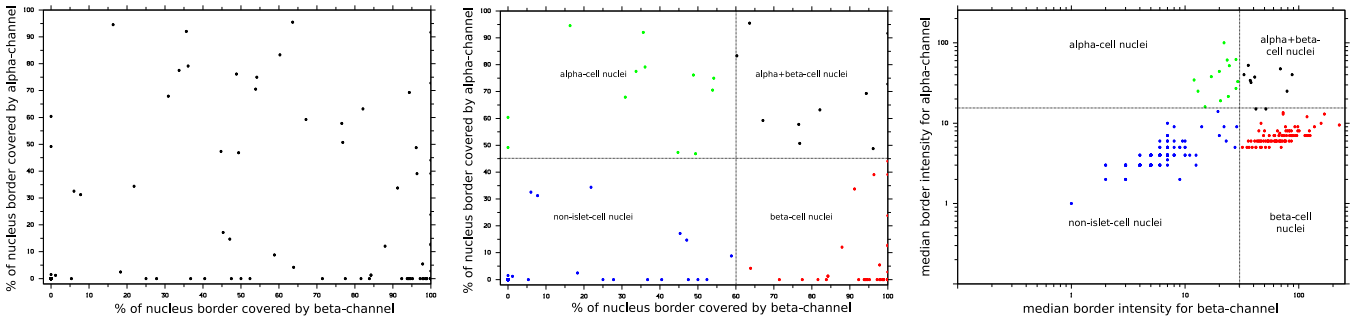

Fig. 7. (a) % of nucleus border covered by α-channel vs. % of nucleus border covered by β-channel for each nucleus. (b) Applying a coverage-threshold of 45% for the α-channel and 60 for the β-channel, the nuclei are classified into 4 classes (non-islet-cell nucleus, α-cell nucleus, β-cell nucleus and both α- and β-cell nucleus). (c) Median nucleus border intensity for α-channel vs. β-channel median nucleus border intensity with logarithmic scaling. Setting a threshold of 30 for the β-channel and 15 for the α-channel separates the nuclei into 4 nucleus classes.

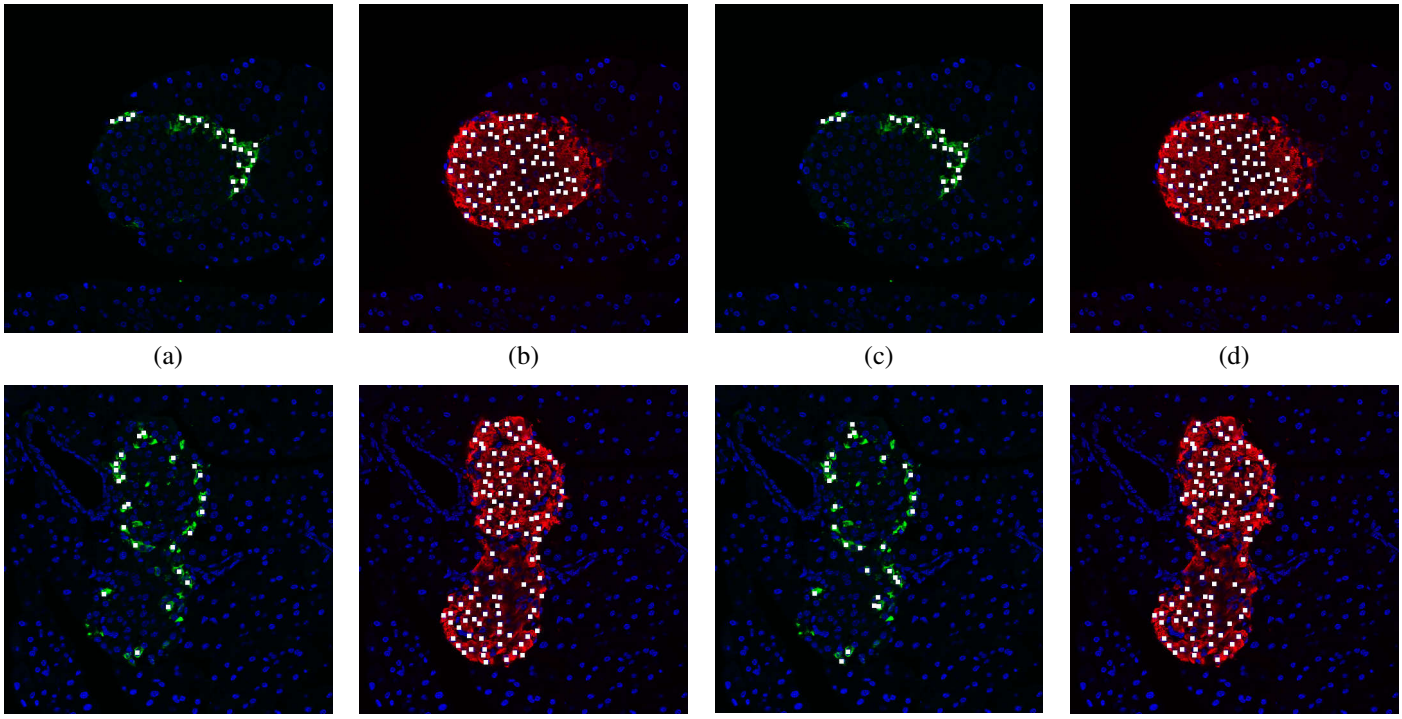

Fig. 8. α- and β-cell nucleus classification results for tissue sample 1 (a)-(d) and 2 (e)-(h). Nuclei assigned to the specific class are marked with a white rectangle. (a)+(e) α-cell nuclei and (b)+(f) β-cell nuclei identified with the border coverage strategy. (c)+(g) α-cell nuclei and (d)+(h) β-cell nuclei identified with median border intensity strategy.

makes high-throughput analysis feasible and provides valuable information for diabetes study.

REFERENCES

[1] V. Starkuviene and R. Pepperkok, "The potential of high-content high-throughput microscopy in drug discovery.," *Br J Pharmacol*, vol. 152, no. 1, pp. 62–71, Sep 2007.

[2] S.G. Megason and S.E. Fraser, "Imaging in systems biology.," *Cell*, vol. 130, no. 5, pp. 784–795, Sep 2007.

[3] Z.E Perlman, M.D. Slack, Y. Feng, T.J. Mitchison, L.F. Wu, and S.J. Altschuler, "Multidimensional drug profiling by automated microscopy.," *Science*, vol. 306, no. 5699, pp. 1194–1198, Nov 2004.

[4] W. Schubert, B. Bonnekoh, A.J. Pommer, L. Philipsen, R. Bckelmann, Y. Malykh, H. Gollnick, M. Friedenberger, M. Bode, and A.W.M. Dress, "Analyzing proteome topology and function by automated multidimensional fluorescence microscopy.," *Nat Biotechnol*, vol. 24, no. 10, pp. 1270–1278, Oct 2006.

[5] V.N. Vapnik, *The Nature of Statistical Learning Theory*, Springer Verlag New York, 1996.

[6] J. Herold, M. Friedenberger, M. Bode, N. Rajpoot, W. Schubert, and T.W. Nattkemper, "Flexible synapse detection in fluorescence micrographs by modeling human expert grading," in *Proc. of 2008 IEEE International Symposium on Biomedical Imaging (ISBI)*, Paris, 2008.

[7] K. Huang and R.F. Murphy, "From quantitative microscopy to automated image understanding.," *J Biomed Opt*, vol. 9, no. 5, pp. 893–912, 2004.

[8] C. Tomasi and R. Manduchi, "Bilateral filtering for gray and color images," in *ICCV*, 1998, pp. 839–46.

[9] N. Otsu, "A threshold selection method from gray-level histograms," *IEEE Transaction on Systems, Man, and Cybernetics*, vol. 9, pp. 62–66, 1979.